Reconstruction of global surface ocean pCO_2 using region-specific predictors based on a stepwise FFNN regression algorithm

Guorong Zhong[1,2,3,4], Xuegang Li[1,2,3,4*], Jinming Song[1,2,3,4*], Baoxiao Qu[1,3,4], Fan Wang[1,2,3,4], Yanjun Wang[1,4], Bin Zhang[1,4], Xiaoxia Sun[1,2,3,4], Wuchang Zhang[1,3,4], Zhenyan Wang[1,3,4], Jun Ma[1,3,4], Huamao Yuan[1,2,3,4], Liqin Duan[1,2,3,4]

[1]Institute of Oceanology, Chinese Academy of Sciences, Qingdao 266071, China
[2]University of Chinese Academy of Sciences, Beijing 101407, China
[3]Pilot National Laboratory for Marine Science and Technology, Qingdao 266237, China
[4]Center for Ocean Mega-Science, Chinese Academy of Sciences, Qingdao 266071, China

Correspondence to: Xuegang Li (lixuegang@qdio.ac.cn); Jinming Song (jmsong@qdio.ac.cn)

Abstract: Various machine learning methods were attempted in the global mapping of surface ocean partial pressure of CO_2 (pCO_2) to reduce the uncertainty of global ocean CO_2 sink estimate due to undersampling of pCO_2. In previous research, the predictors of pCO_2 were usually selected empirically based on theoretic drivers of surface ocean pCO_2, and the same combination of predictors was applied in all areas unless lack of coverage. However, the differences between the drivers of surface ocean pCO_2 in different regions were not considered. In this work, we combined the stepwise regression algorithm and a Feed-Forward Neural Network (FFNN) to select predictors of pCO_2 based on the mean absolute error in each of the 11 biogeochemical provinces defined by the Self-Organizing Map (SOM) method. Based on the predictors selected, a monthly global 1° × 1° surface ocean pCO_2 product from January 1992 to August 2019 was constructed. Validation of different combinations of predictors based on the SOCAT dataset version 2020 and independent observations from time-series stations was carried out. The prediction of pCO_2 based on region-specific predictors selected by the stepwise FFNN algorithm was more precise than that based on predictors from previous researches. Applying the FFNN size improving algorithm in each province decreased the mean absolute error (MAE) of the global estimate to 11.32 μatm and the root mean square error (RMSE) to 17.99 μatm. The script file of the stepwise FFNN algorithm and pCO_2 product are distributed through the Institute of Oceanology of the Chinese Academy of Sciences Marine Science Data Center (IOCAS; http://dx.doi.org/10.12157/iocas.2021.0022, Zhong et al., 2021).

1 Introduction

As a net sink for atmospheric CO_2, global oceans have removed about one-third of anthropogenic CO_2 since the beginning of the industrial revolution (Sabine et al., 2004; Friedlingstein et al., 2019). However, the global ocean sea-air CO_2 flux averaged between 2001-2015 varies from -1.55 to -1.74 PgC yr^{-1} with the maximum difference in individual years nearly 0.6 PgC yr^{-1}, depending on the surface ocean partial pressure of CO_2 (pCO_2) product. These differences largely stem from differences in pCO_2 estimates across the products (Rödenbeck et al., 2014; Iida et al., 2015; Landschützer et al., 2014; Denvil-Sommer et al., 2019). The magnitude and direction of the flux are primarily set by the air-sea pCO_2 difference. Surface water pCO_2 greater than the overlying air indicates CO_2 is released from the ocean to the air. Conversely, absorption of CO_2 by oceans happens when the pCO_2 of the surface water is lower than the overlying air. The ocean in these two scenarios is known as oceanic carbon source and oceanic carbon sink, respectively.

Sparse and uneven observations of surface ocean pCO_2 in time and space severely limited the understanding of interannual variability of oceanic carbon sink, and researches based on different methods were carried out to break this barrier. In earlier studies, traditional unitary and multiple regression methods between surface ocean pCO_2 and its drivers were attempted in the mapping of surface ocean pCO_2, which were limited in specific regions and sometimes even in particular seasons with a relatively high root mean square error (RMSE) (Sarma et al., 2006; Takahashi et al., 2006; Shadwick et al., 2010; Chen et al., 2011; Marrec et al., 2015). Advances in artificial neural networks and other machine learning algorithms, such as the feed-forward neural network (FFNN) method (Zeng et al., 2014; Zeng et al., 2015; Moussa et al., 2016; Denvil-Sommer et al., 2019) and self-organization mapping (SOM) method (Friedrich and Oschlies, 2009; Telszewski et al., 2009; Hales et al., 2012; Nakaoka et al., 2013), significantly reduced the bias in the interpolation based on relationships between surface ocean pCO_2 and its drivers. In addition, finding better predictors or combining SOM with other neural networks was also attempted to decrease the pCO_2 predicting error further (Hales et al., 2012; Nakaoka et al., 2013; Landschützer et al., 2014; Chen et al., 2019; Denvil-Sommer et al., 2019; Zhong et al., 2020; Wang et al., 2021). However, the selection of predictors in the surface ocean pCO_2 mapping was more empirical, focusing on the theoretical drivers of the pCO_2 and its variation. Sea surface temperature and salinity, related to the solubility of CO_2 in seawater, are considered as the most important and used in almost all related studies (Landschützer et al., 2013;

Nakaoka et al., 2013; Moussa et al., 2016; Laruelle et al., 2017; Zeng et al., 2017; Denvil-Sommer et al., 2019). Similarly, the chlorophyll-a concentration is also widely used (Nakaoka et al., 2013; Landschützer et al., 2014; Laruelle et al., 2017; Zeng et al., 2017; Denvil-Sommer et al., 2019), which is related to the phytoplankton uptake of CO_2. One more predictor, mixed layer depth, frequently appears in associated studies as a proxy related to the vertical transport of dissolved carbon (Telszewski et al., 2009; Nakaoka et al., 2013; Landschützer et al., 2014; Zeng et al., 2017; Denvil-Sommer et al., 2019). In addition, sampling information, such as latitude and longitude (Friedrich and Oschlies, 2009; Jo et al., 2012; Zeng et al., 2015; Zeng et al., 2017; Denvil-Sommer et al., 2019; Gregor et al. 2019) and sampling time (Friedrich and Oschlies, 2009; Zeng et al., 2015), has been used as a predictor. In recent research, the dry air mixing ratio of atmospheric CO_2 (xCO_2), related to the CO_2 level in the air, was also used to predict surface ocean pCO_2 (Landschützer et al., 2014; Denvil-Sommer et al., 2019). The sea surface height, which was considered effective in improving the spatial pattern and the accuracy of surface ocean pCO_2 mapping at the basin and regional scale, and the monthly anomalies of the most widely used predictors mentioned above were used by the Denvil-Sommer et al. (2019). In the research focusing on the surface ocean pCO_2 mapping of coastal areas, the bathymetry, sea ice, and wind speed were also used as predictors (Laruelle et al., 2017). In each of these researches, the same combination of predictors was applied in all global ocean areas, although the global ocean was divided into several biogeochemical provinces in some of the researches. However, the predictor that plays a vital role in the surface ocean pCO_2 reconstruction at one region may not be a good predictor of surface ocean pCO_2 in the other regions due to complex and variable drivers. Nevertheless, no widely recognized methods for judging the importance of each predictor in the surface ocean pCO_2 mapping are available yet. Thus, we attempted to construct a stepwise FFNN algorithm to rank the importance of predictors and figure out the optimal combination in each biogeochemical province defined by SOM for decreasing the prediction errors in the surface ocean pCO_2 mapping.

2 Methodology

2.1 Data

The surface ocean fugacity of CO_2 (fCO_2) observation data from the Surface Ocean CO_2 Atlas fCO_2 dataset version 2020 (SOCATv2020) (Bakker et al., 2016) was used to construct the non-linear relationship between surface ocean pCO_2 and predictors. The conversion between fCO_2 and pCO_2 was following the formula (Körtzinger, 1999)：

$$fCO_2 = pCO_2 \cdot exp\left(P \cdot \frac{B+2\delta}{RT}\right) \quad (1)$$

where fCO_2 and pCO_2 are in micro-atmospheres (μatm), P is the total atmospheric surface pressure (Pa) using the National Centers for Environmental Prediction (NCEP) monthly mean sea level pressure product (Dee et al., 2011), and T is the absolute temperature (K). R is the gas constant (8.314 J K^{-1} mol^{-1}). Parameters B (m^3 mol^{-1}) and δ (m^3 mol^{-1}) are both viral coefficients (Weiss, 1974).

In this work, 33 predictors were used (Table 1), where 21 were chosen from previous researches of surface ocean pCO_2 reconstruction based on machine learning methods. In addition, 12 predictors which were only used in similar previous research focused on the mapping of total alkalinity or dissolved inorganic carbon (Broullón et al., 2019; Broullón et al., 2020), or were possibly related to the driver of surface ocean pCO_2 and its variability, were selected to be tested (Predictors with the * label in Table 1). Most of these products were retrieved at 1° × 1° resolution. Some products retrieved at higher resolution were downscaled to 1° × 1° resolution by taking the average of all values in each 1° × 1° grid.

Table 1. Predictors and corresponding data products

Predictor	Abbreviation	Data product	Resolution
Sine of latitude	sLat	-	-
Sine of longitude	sLon	-	-
Cosine of longitude	cLon	-	-
Number of months since January 1992	N_{mon}	-	-
Year	Year	-	-
Month	Month	-	-
Sea surface temperature	SST	Chen et al., 2016; Chen et al., 2017	1°× 1°, monthly, 1940-2021
Monthly anomaly of SST	SST_{anom}	Chen et al., 2016; Chen et al., 2017	1°× 1°, monthly, 1940-2021
Sea surface salinity	SSS	Chen et al., 2020	1°× 1°, monthly, 1940-2021
Monthly anomaly of SSS	SSS_{anom}	Chen et al., 2020	1°× 1°, monthly, 1940-2021
Mixed layer depth	MLD	Menemenlis et al., 2008	0.25°× 0.25°, monthly, 1992-2019
Monthly anomaly of MLD	MLD_{anom}	Menemenlis et al., 2008	0.25°× 0.25°, monthly, 1992-2019
Sea surface height	SSH	Menemenlis et al., 2008	0.25°× 0.25°, monthly, 1992-2019
Monthly anomaly of SSH	SSH_{anom}	Menemenlis et al., 2008	0.25°× 0.25°, monthly, 1992-2019

Sea ice fraction	f_{ice}	Dee et al., 2011	1°× 1°, monthly, 1979-2019
10 m Wind speed	Wind	Dee et al., 2011	1°× 1°, monthly, 1979-2019
Dry air mixing ratio of atmospheric CO_2	xCO_2	GLOBALVIEW-CO2, 2011	0.25° latitude, monthly, 1979-2019
Monthly anomaly of xCO_2	$xCO_{2\ anom}$	GLOBALVIEW-CO2, 2011	0.25° latitude, monthly, 1979-2019
Bathymetry	Bathymetry	Commerce et al., 2006	2'× 2'
Chlorophyll concentration	Chl-a	NASA Ocean Biology Processing Group, 2018	9km×9km, monthly, 2002-2021
Monthly anomaly of CHL	Chl-a $_{anom}$	NASA Ocean Biology Processing Group, 2018	9km×9km, monthly, 2002-2021
W velocity of ocean currents at 5 m depth*	W_{vel}(5m)	Menemenlis et al., 2008	0.25°× 0.25°, monthly, 1992-2019
W_{vel} at 65 m depth*	W_{vel}(65m)	Menemenlis et al., 2008	0.25°× 0.25°, monthly, 1992-2019
W_{vel} at 105 m depth*	W_{vel}(105m)	Menemenlis et al., 2008	0.25°× 0.25°, monthly, 1992-2019
W_{vel} at 195 m depth*	W_{vel}(195m)	Menemenlis et al., 2008	0.25°× 0.25°, monthly, 1992-2019
Sea level pressure*	SLP	Dee et al., 2011	1°× 1°, monthly, 1979-2019
Surface pressure*	Surface pressure	Dee et al., 2011	1°× 1°, monthly, 1979-2019
Climatology of dissolved oxygen*	DO	Garcia et al., 2019b	1°× 1° in the horizontal, 102 depth levels (0–5500 m) in the vertical and monthly
Climatology of nitrate*	Nitrate	Garcia et al., 2019a	1°× 1° in the horizontal, 102 depth levels (0–5500 m) in the vertical and monthly
Climatology of phosphate*	Phosphate	Garcia et al., 2019a	1°× 1° in the horizontal, 102 depth levels (0–5500 m) in the vertical and monthly
Climatology of silicate*	Silicate	Garcia et al., 2019a	1°× 1° in the horizontal, 102 depth levels (0–5500 m) in the vertical and monthly
Oceanic Nino Index*	ONI	Huang et al., 2017	Monthly, 1950-2021
Southern Hemisphere Annular Mode Index*	SAM	Marshall, G. J., 2003	Monthly, 1957-2021

(Predictors with the * label were first included in the pCO_2 mapping, where the climatology of nitrate, phosphate, silicate, and dissolved oxygen were used in the mapping of total alkalinity and dissolved inorganic carbon in previous research. All data products retrieved at the resolution higher than 1°× 1° were downscaled to 1° × 1° resolution.)

2.2 Biogeochemical provinces defined by the Self-Organizing Map

For applying a different combination of predictors in regions based on the differences in the dominated drivers of pCO_2 and its variability, the global ocean was divided into a set of biogeochemical provinces using a Self-Organizing Map (SOM) method. The monthly climatology of temperature, salinity, mixed layer depth, sea surface height, nitrate, phosphate, silicate, and dissolved oxygen and pCO_2 climatology from Landschützer et al. (2020) were put into a 3-by-4 size SOM network to generate 12 biogeochemical provinces, where the monthly climatology data in all 12 months were put into one SOM network to generate one discrete set of biogeochemical provinces. Provinces with less than 10 pixels and less than 1000 SOCAT observations were defined as discrete small "island" provinces and then merged with nearest provinces. The provinces covering areas separated by land were further divided artificially. For example, the province covering the north subtropical Pacific and the province covering the north subtropical Atlantic was set as one province in the original output of SOM, but it was mainly separated by the North American continent. So, we divided the province into two new provinces. The final version includes 11 biogeochemical provinces. In this study, the coastal area was not involved, and the boundary was defined as 200 m depth. In addition, the pCO_2 mapping based on SOM-defined provinces tends to be less smooth near the border of different biogeochemical provinces, with an obvious borderline appearing. However, applying different predictors may make this problem worse. To obtain a smoother distribution, we defined the area within five 1x1 grids of province boundaries as a "boundary area". Samples in the boundary area will be used as training samples in all adjacent provinces (Fig. S1). But this definition does not change the actual spatial coverage of each province, only bringing more training samples near the province boundary.

2.3 Stepwise FFNN algorithm

For finding a better combination of pCO_2 predictors, a stepwise Feed-forward neural networks (FFNN) algorithm was constructed. The FFNN comprises four parts: input, hidden, summation, and output layer (Fig. 1). The input layer is designed to pass the inputs to the hidden layer, and the number of neurons is equal to the dimensions of the input matrix p. The hidden layer includes 25 neurons in the FFNN model, with a tan-sigmoid function as the transfer function. The input p is multiplied by a matrix of weights (w_1 in Fig. 1), and the inner product between the result and a bias matrix (b_1 in Fig. 1) is calculated as the input of the transfer function in the first hidden layer. In the summation layer, the transfer function f_2 is a linear function. The output of the hidden

layer is multiplied by another matrix of weights and summed. All bias and weights matrixes were randomly assigned at the beginning of FFNN training. The randomly assigned bias and weights matrixes, the number of training samples, and the sort order of training samples in the input matrix *p* define where the FFNN starts training in errors space. The practice of FFNN changes when these conditions change. Here we fixed the training samples and set one constant random number stream in MATLAB to ensure that the difference between the MAE based on different predictors entirely stems from the predictor differences. The random number was randomly chosen. When using different random number streams, several predictors at the end of the output list of the stepwise FFNN algorithm differed. However, the leading predictors were consistent, and the different predictors were also related. The fixed random number makes all networks using different predictors start training from the same point at the error space when comparing the performance of each predictor.

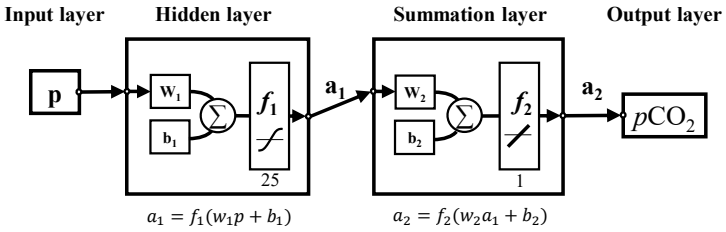

Figure 1. The structure of feed-forward neural network. **p**: input matrix; **w**: weighted matrix; **b**: bias matrix; ∑: sum; $\boldsymbol{f_1}$: tan-sigmoid transfer function; $\boldsymbol{f_2}$: linear function; **a**: output matrix.

In the stepwise part, predictors of pCO_2 are going to be added and removed one by one, and which predictors will be finally used in the pCO_2 predicting is determined according to the real-time change of predicting error. The mean absolute error (MAE), calculated using a K-fold cross validation method, was used to estimate the performance of each predictor in the FFNN predicting. Although the Root-Mean-Squared Error (RMSE) was widely used for the validation of machine learning methods, compared to the MAE, the RMSE was more sensitive to a few extreme samples, which were generally deviated far from the FFNN predicting values, resulting in a considerable discrepancy between the FFNN outputs and pCO_2 observations sometimes up to hundreds of μatm. A higher weight might be put on these few extreme samples than other samples in the predictor selection if the performance of each predictor was estimated by RMSE in the stepwise FFNN algorithm. To avoid the higher weight on these few extreme samples, the MAE was used instead for the internal performance loss function in the stepwise FFNN algorithm. The basic principle of the stepwise FFNN algorithm was adding each predictor from a set of predictors into the inputs of FFNN

and removing each redundant predictor from the inputs successively to reduce the MAE in the fastest way, until no decrease in the MAE appeared (Fig. 2), where the predictor having no contribution to the reducing of prediction error was considered as redundant.

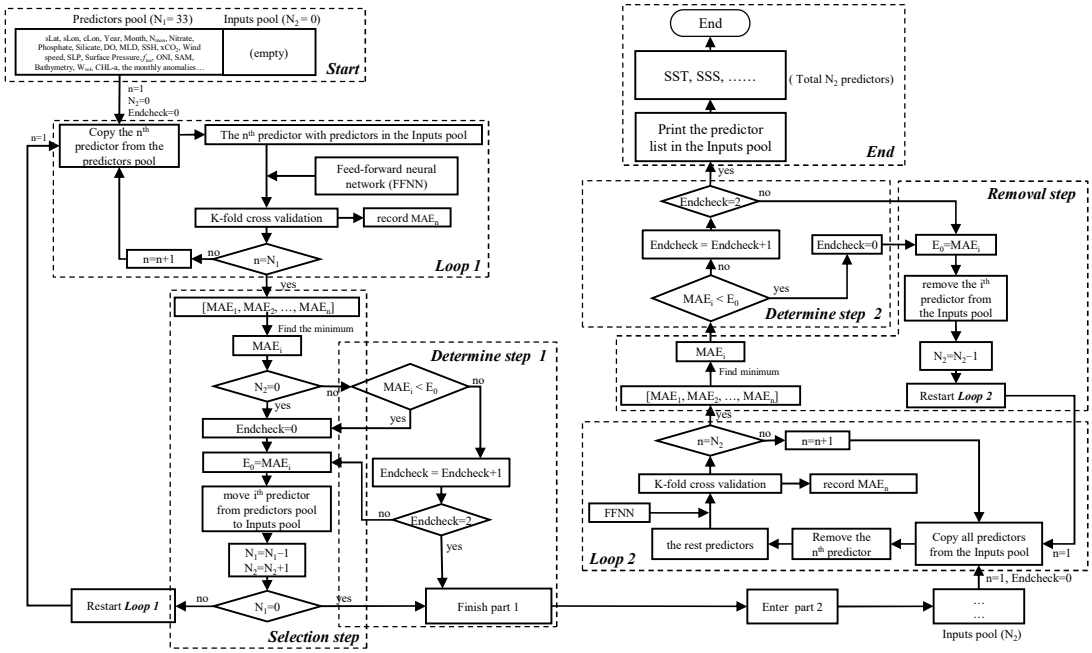

Figure 2. The procedure of the stepwise FFNN algorithm. The flowchart follows an order of "left top – left bottom – right bottom – right top". The meaning of *Predictors pool*: store all predictors waiting to be tested; *Inputs pool*: store predictors that were temporally considered as good predictors; *Loop 1* and *Loop 2*: calculate the MAE when each predictor was added or removed; *Selection step*: add good predictors to the *Inputs pool*; *Removal step*: remove predictors from the Inputs pool if removing lead to MAE decrease; *Determine step*: check if the process reach end condition. N_1 and N_2: number of predictors in the *Predictors pool* and *Inputs pool*, respectively; E_0: lowest MAE in the last iteration of *Loop 1* or *Loop 2*; *Endcheck*: the number of iterations that E_0 continuously increased.

At the beginning of the stepwise FFNN algorithm, all available predictors were put into a matrix, referred to as *Predictors pool* (*Start* in Fig. 2). Each row represents one predictor, and each column represents one SOCAT sample. In this work, we collected 33 predictors for the test, that is, the *Predictors pool* matrix has 33 rows. Meanwhile, a matrix referred to as *Inputs pool* (*Start* in Fig. 2) was set up to store predictors with good performance, where good performance means that adding these predictors can significantly decrease the MAE between SOCAT pCO_2 measurements and FFNN pCO_2 predictions. Then a loop of K-fold validation test ran out to calculate the MAE when predicting pCO_2 by each predictor in the *Predictors pool* in the first step (*Loop 1* in Fig. 2). Thus 33 MAE values were obtained totally, and the minimum was

recorded as E_0. The predictor corresponding to the minimum MAE value was moved from the *Predictors pool* to the *Inputs pool* (*Selection step* in Fig. 2). After that, the *Loop 1* restarted, i.e., the second step started with one predictor removed to the inputs pool and the rest 32 predictors waiting to be tested. Then, the pCO_2 was predicted using each of the rest 32 predictors in the predictors pool with the addition of all predictors in the inputs pool, and 32 MAE values were calculated out. If the MAE in the lowest situation, represented by the MAE_i, decreased compared to the E_0, the i^{th} predictor was considered a good predictor and moved from the predictors pool to the inputs pool. Then the value of E_0 was replaced by the MAE_i (*Selection step* in Fig. 2). The part 1, including *Loop 1*, *Selection step,* and *Determine step 1* in Fig. 2, was repeated until no predictor was left in the *Predictors pool* or no decrease of E_0 can be found no matter which two predictors were added in the next two steps. At this time, the part 1 of the stepwise FFNN algorithm finished, and all predictors left in the *Predictors pool* were considered redundant. The second part ran in the opposite way that the predictors were removed from the *Inputs pool* one by one to decrease E_0 the fastest (*Loop 2* in Fig. 2). The second part was aimed to remove the predictor that can be represented by other predictors in the inputs pool (*Removal step* in Fig. 2) and finished in the similar condition that no significant decrease can be found no matter which predictor was removed in the next two steps (*Determine step 2* in Fig. 2).

2.4 pCO_2 product

Dataset of predictors except for Chl-a start since 1992 or earlier, while Chl-a data ranges from August 2002 to the present. In each province, the stepwise FFNN algorithm was run out once first based on all samples covered by Chl-a data; then the algorithm was run out secondly based on samples and all predictors except Chl-a and Chl-a $_{anom}$ in the year that Chl-a gridded data was not available. The pCO_2 mapping in the year that Chl-a gridded data was not available was carried out based on the predictors selected in the second run. Then the final product was built based on two FFNNs, one trained for the period from August 2002 to August 2019 using one predictor set including Chl-a or Chl-a $_{anom}$, and the second one for the period from January 1992 to July 2002 using the second predictor set without Chl-a and Chl-a $_{anom}$. Although the performance may improve with the number of neurons increasing, the influence of the number of neurons on the performance of FFNN pCO_2 prediction remains unclear. To further decrease the predicting error between FFNN outputs and SOCAT measurements, the number of neurons was improved by an error test in each province. The number of neurons increased from 5 to 300 (the increment was five during 5-50 and ten during 50-

100 and fifty during 100-300). Then the corresponding MAE values of each size were recorded, and the number of neurons with the lowest MAE was applied. This test avoided the appearance of insufficient learning capacity for complex nonlinear relationships due to too few neurons and the overfitting problem due to too many neurons. Finally, based on the predictors selected by the stepwise FFNN algorithm and improved FFNN size, a monthly global 1°×1° surface ocean pCO_2 product from January 1992 to August 2019 was constructed.

2.5 Validation

To better estimate the predicting error of FFNN, the MAE and the RMSE, which were widely used in previous research, were calculated using a K-fold cross validation method. To avoid overfitting caused by a lack of independence between the training and testing samples, we put the SOCAT samples in chronological order and then divided them into the group of years (Fig. 1) (Gregor et al., 2019). In this paper, the value of K was set as 4. Thus, among every four neighboring years, three group samples were used to train the FFNN model, and the rest was used for testing. Total 4 iterations were carried out, where testing year changed in each iteration. After 4 iterations finished, all samples were used for testing only once, and the MAE and RMSE between FFNN output and the testing samples were calculated. The performance of the predictor selection algorithm was estimated by comparing the MAE and RMSE results of the FFNN based on predictors selected by the stepwise FFNN algorithm with the result based on predictors used in previous researches in each biogeochemical province (Table 2). All validation groups were applied with the same FFNN and same samples from SOCAT, with the only differences in predictors. The same K-fold validation procedure was applied for three validation groups based on different pCO_2 predictors. Thus, three results were generated to estimate whether the stepwise FFNN algorithm can effectively find a better combination of pCO_2 predictors. Finally, the pCO_2 data generated in all validation groups were further compared with the completely independent observations from the Hawaii Ocean Time-series (HOT, 22° 45'N, 158° 00'W, since October 1988) (Dore et al., 2009), Bermuda Atlantic Time-series Study (BATS, 31°50'N, 64°10'W, since October 1988) (Bates, 2007) and The European Station for Time Series in the Ocean Canary Islands (ESTOC, 29°10'N, 15°30'W, from 1995 to 2009) (González-Dávila and Santana-Casiano, 2009) time-series station. The pCO_2 at HOT and BAT were estimated from TA and DIC, and pCO_2 at ESTOC were directly measured. These observations were not included in the SOCAT dataset.

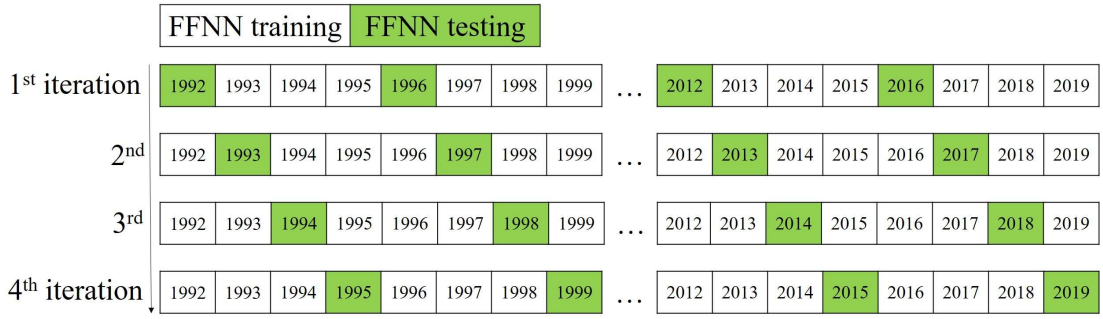

Figure 3. The procedure of K-fold validation. (The K value was set as 4, so iterations repeated four times until all samples were set as testing samples once. In each iteration, samples in 7 years were set as testing samples (green cells) and in the rest 21 years as training samples (white cells) to increase the independence.)

Table 2. Validation group using different predictors

Validation group	Predictor
FFNN1	Predictors selected by stepwise FFNN algorithm
FFNN2	SST, SSS, $\log_{10}$(MLD), Chl-a, xCO_2, SST_{anom}, SSS_{anom}, $xCO_{2\ anom}$, Chl-a $_{anom}$, $\log_{10}$(MLD) $_{anom}$ (Landschützer et al., 2014)
FFNN3	SST, SSS, SSH, MLD, xCO_2, Chl-a, SSS_{anom}, SST_{anom}, SSH_{anom}, Chl-a $_{anom}$, MLD_{anom}, $xCO_{2\ anom}$, sLat, sLon, cLon (Denvil-Sommer et al., 2019)

(The FFNN performance of three groups with different predictors of pCO_2 were compared to test the result of stepwise FFNN algorithm. Predictors in the group FFNN1 were selected using stepwise FFNN algorithm, and predictors in the group FFNN2 were selected from Landschützer et al. (2014), and in the group FFNN3 from Denvil-Sommer et al. (2019).)

3 Results and discussion

3.1 Biogeochemical provinces and corresponding predictors of pCO_2

11 biogeochemical provinces generated from the SOM method after the separated small 'island' was removed and the province separated by lands was divided manually (Fig. 4). The results of the stepwise FFNN algorithm in each province are shown in Table 3. The predictors were listed in the order that the stepwise FFNN algorithm printed recommended predictors out. The predictor printed earlier was relatively more recommended and played an important role in predicting pCO_2 based on FFNN. Applying these predictors effectively decreased the predicting error between the FFNN outputs and pCO_2 values from validation samples. Thus it is reasonable to consider that these predictors were highly related to the drivers of pCO_2 and its variability. Predictors

representing sampling positions were also listed as recommended predictors in some provinces, including latitude, longitude, and sampling time, suggesting that relatively steady spatial or temporal variability patterns of surface ocean pCO_2 existed in these biogeochemical provinces. For example, the predictor month was considered recommended in most provinces, especially P4 subpolar Atlantic and P5 north subtropical Atlantic. While pCO_2 in these areas regularly peaked and bottomed out in summer and winter (Takahashi et al., 2009; Landschützer et al., 2016; Landschützer et al., 2020). Similarly, the sine of latitude and the sine and cosine of longitude were listed as recommended predictors of pCO_2 in most provinces, suggesting a meridional or zonal uniformly varying spatial distribution pattern of pCO_2, which was not learned sufficiently by the FFNN model from existing measured predictors and the predictors related to the spatial position were applied as supplementary.

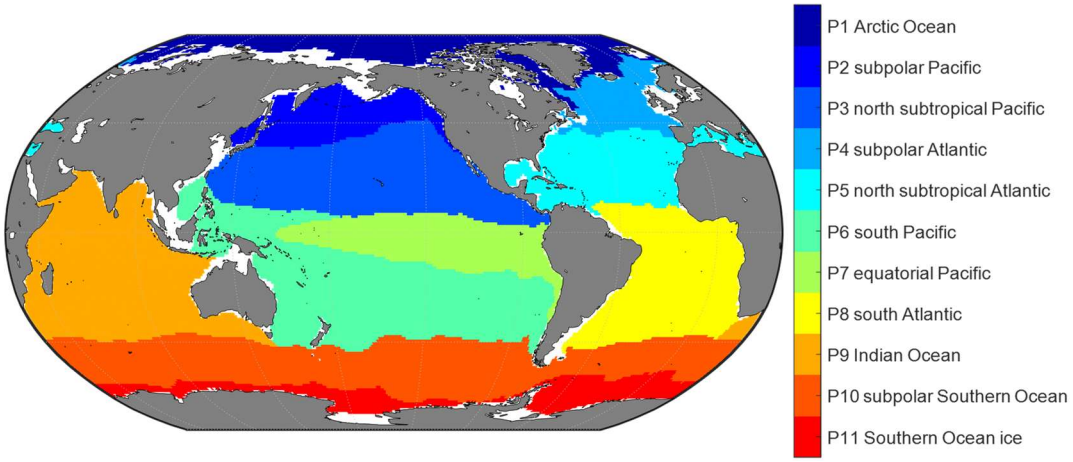

Figure 4. The map of biogeochemical provinces based on SOM.

As basic predictors highly related to the ocean environment, the temperature and salinity was considered as parts of the most important predictors of surface ocean pCO_2 and was applied in the pCO_2 prediction in almost all previous relating researches based on various method (Jo et al., 2012; Signorini et al., 2013; Landschützer et al., 2014; Marrec et al., 2015; Chen et al., 2016; Moussa et al., 2016; Chen et al., 2017; Laruelle et al., 2017; Zeng et al., 2017; Chen et al., 2019; Denvil-Sommer et al., 2019). The results of the stepwise FFNN algorithm also supported this. The temperature was listed as a recommended predictor in all biogeochemical provinces, suggesting that temperature was one of the most critical drivers of pCO_2 and its variability in these provinces. Similarly, results from the stepwise FFNN algorithm provide evidence for the importance of salinity in predicting pCO_2, which was also listed as a predictor in most provinces. The dry air mixing ratio of atmospheric CO_2 (xCO_2) and the monthly

anomaly of xCO_2 were also recommended predictors in most biogeochemical provinces, suggesting that the exchange of CO_2 across the sea-air interface was also an important driver of surface ocean pCO_2. As a widely used predictor in the pCO_2 prediction, the chlorophyll-a concentration (Chl-a) played an essential role in fitting the influence of biological activities on pCO_2 in previous researches (Landschützer et al., 2014; Zeng et al., 2017; Laruelle et al., 2017; Denvil-Sommer et al., 2019). Especially in the province P10 subpolar Southern Ocean and P11Southern Ocean ice, the Chl-a was listed as the most recommended predictor in the result of the stepwise FFNN algorithm. While in some other provinces (P1 Arctic Ocean and P5 north subtropical Atlantic), the Chl-a was considered redundant that no effective decrease of MAE between FFNN outputs and pCO_2 measurements appeared when Chl-a data was used. Similar to the period that Chl-a was not available (represented by the subscript 'b'), the phosphate, nitrate, silicate, or dissolved oxygen were recommended instead. In the province P1 Arctic Ocean, the silicate concentration and temperature were considered the most crucial predictor of pCO_2.

Table 3. Predictors in each biogeochemical province

Province	Predictors in the order of the stepwise FFNN algorithm output
P1 Arctic Ocean	Silicate, SST, Wind speed, SSS, $\log_{10}$(MLD), SSS_{anom}, sLat, month, W_{vel}(65m), $\log_{10}(MLD)_{anom}$, xCO_2, cLon, Bathymetry, SSH
P2 subpolar Pacific $_a$*	Nitrate, Chl-a, SSS, xCO_2, cLon, SST, $\log_{10}$(MLD), sLon, sLat, month
P2 subpolar Pacific $_b$*	Nitrate, xCO_{2anom}, sLon, SST, sLat, $\log_{10}$(MLD), cLon, SSS, SSH_{anom}, DO, W_{vel}(195m), Bathymetry, Silicate
P3 north subtropical Pacific $_a$	$\log_{10}$(MLD), N_{mon}, SSH, SST, sLon, sLat, SSS, Bathymetry, month, $\log_{10}(MLD)_{anom}$, cLon, Surface pressure, W_{vel}(105m), Chl-a, DO, SSH_{anom}, $xCO_{2\ anom}$
P3 north subtropical Pacific $_b$	$\log_{10}$(MLD), xCO_2, sLat, sLon, SST, Surface pressure, cLon, SSS, W_{vel}(5m), N_{mon}, $\log_{10}(MLD)_{anom}$, month, Phosphate, $xCO_{2\ anom}$, W_{vel}(105m)
P4 subpolar Atlantic $_a$	month, sLat, cLon, SST, Year, Chl-a, DO, SSS_{anom}, W_{vel}(195m), SSH, $\log_{10}$(MLD), Bathymetry, SSS
P4 subpolar Atlantic $_b$	month, xCO_2, DO, Wind speed, $\log_{10}$(MLD), W_{vel}(195m), sLon, Bathymetry, W_{vel}(5m), SST, Phosphate, Year, N_{mon}
P5 north subtropical Atlantic	month, Year, SST, sLon, sLat, SSS, SST_{anom}, SSH, Bathymetry, W_{vel}(5m), cLon, W_{vel}(65m), $\log_{10}(MLD)_{anom}$
P6 south Pacific $_a$	SST, sLon, $xCO_{2\ anom}$, sLat, SSS, month, Phosphate, Chl-a, Chl-a_{anom}, W_{vel}(65m), $\log_{10}$(MLD), $\log_{10}(MLD)_{anom}$, Nitrate, Bathymetry

P6 south Pacific $_b$	xCO_2, sLat, SSS, SST, Phosphate, SLP, $xCO_{2\ anom}$, sLon, cLon, W_{vel}(105m), W_{vel}(65m), DO, Bathymetry, SSH, SAM
P7$_a$ equatorial Pacific	Nitrate, xCO_2, sLat, SSS, SST, cLon, $xCO_{2\ anom}$, log_{10}(MLD), sLon, Chl-a, Phosphate, W_{vel}(5m), W_{vel}(105m), W_{vel}(195m)
P7$_b$ equatorial Pacific	SST, SSS, Year, sLat, month, cLon, SSH, Bathymetry, W_{vel}(65m), xCO_2
P8 south Atlantic $_a$	sLat, $xCO_{2\ anom}$, SSS, log_{10}(MLD), Chl-a, SSH_{anom}, W_{vel}(195m), cLon, SST, W_{vel}(65m), Bathymetry, Nitrate
P8 south Atlantic $_b$	SST, xCO_2, cLon, sLat, SSS, Silicate, SSH, log_{10}(MLD), sLon
P9 Indian Ocean $_a$	SST, cLon, sLat, Nitrate, W_{vel}(65m), log_{10}(MLD), SLP, Chl-a, Year, $log_{10}(MLD)_{anom}$, SSH_{anom}
P9 Indian Ocean $_b$	SLP, month, sLon, $xCO_{2\ anom}$, SST, Silicate, W_{vel}(65m)
P10 subpolar Southern Ocean $_a$	Chl-a, log_{10}(MLD), N_{mon}, SSS, SST, Bathymetry, SSH_{anom}, W_{vel}(5m), Chl-a $_{anom}$, xCO_2
P10 subpolar Southern Ocean $_b$	Wind speed, $xCO_{2\ anom}$, SSS, Phosphate, log_{10}(MLD), W_{vel}(65m), Bathymetry, SST, month
P11 Southern Ocean ice $_a$	Chl-a, sLon, Bathymetry, SSS, SSH, SST, Nitrate, cLon, sLat
P11 Southern Ocean ice $_b$	month, DO, SST, SSH, sLat, Nitrate, sLon, SSS, W_{vel}(195m), Silicate, SSHanom

*: Due to insufficient coverage of Chl-a data in the polar areas and during the period before 2002, in provinces that Chl-a or Chl-a $_{anom}$ were selected as predictors, the pCO_2 data was divided into two periods. The period with Chl-a data available was represented by the subscript 'a', such as $P2_a$, including global grids from 2002 to 2019 except polar grids in winter. The period with Chl-a data unavailable was represented by the subscript 'b', such as $P2_b$, including global grids from 1992 to 2001 and some polar grids in winter from 1992 to 2019.

3.2 pCO_2 product

Based on the predictors given by the stepwise FFNN algorithm in each biogeochemical province, a FFNN size (representing the number of neurons in the hidden layer) improving validation was applied to decrease the prediction error further. The MAE values based on the same samples and FFNN model with a different number of neurons were calculated, then the number of neurons corresponding to the lowest MAE was applied (Fig. 5a). The MAE in most provinces tends to decrease first and then increase when the number of neurons in the hidden layer of the FFNN model increased from 5 to 300. Based on the variation of MAE with the number of neurons in the FFNN hidden layer, the optimal FFNN size in each province was considered as the number of neurons when the MAE was lowest. The result and corresponding MAE are shown in Fig. 5b. After applying optimal FFNN size in each province, the MAE and

RMSE of global estimates between predicted pCO_2 and measurements from SOCAT v2020 further decreased to 11.32 and 17.99 μatm, respectively.

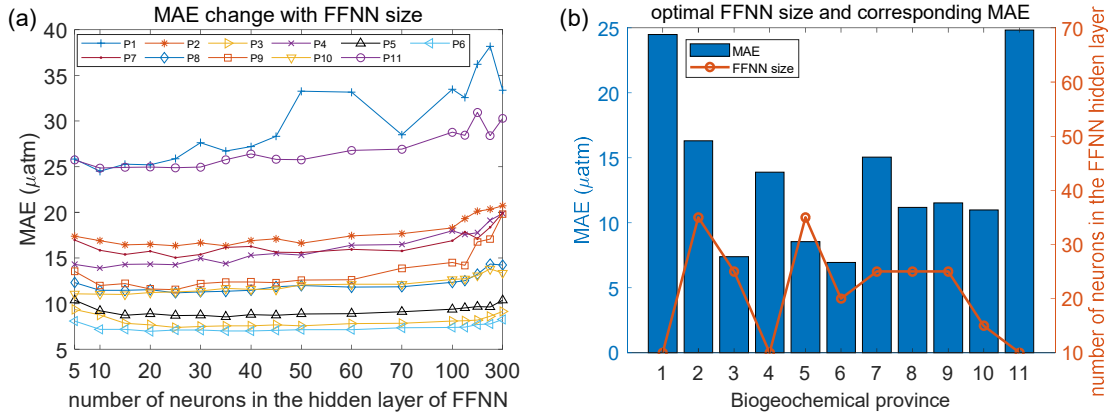

Figure 5. MAE of different FFNN size in each biogeochemical province. a): MAE between predicted pCO_2 and SOCAT observations was calculated using the same samples and FFNN with a different number of neurons. b): the optimal FFNN size refers to the number of neurons when MAE is lowest.

Then the RMSE and mean residuals in each grid were calculated based on the K-fold cross validation method. In most grids, the RMSE was lower than 10 μatm, and the mean residuals was close to zero (Fig. 6). However, the prediction error in the north subpolar Pacific, the eastern equatorial Pacific, and the Southern Ocean near the Antarctic continent was significantly higher than in other areas. Also, the distribution of mean residuals suggested that surface ocean pCO_2 in the Indian Ocean tends to be overestimated by the FFNN models. While in other regions the distribution of mean residuals was more discrete, and no obvious pattern was found.

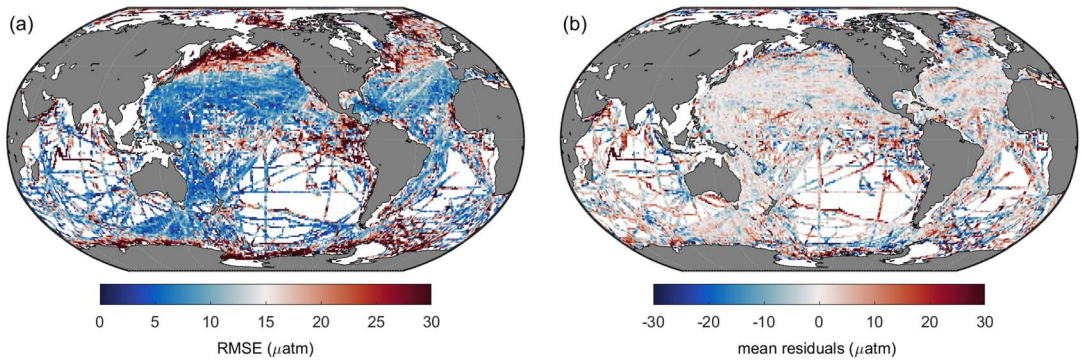

Figure 6. Global maps of (a) RMSE and (b) mean residuals between predicted pCO_2 and SOCAT observations

3.3 Validation of the stepwise FFNN algorithm based on SOCAT samples

Validation based on the K-fold cross validation method suggested that most FFNN outputs were quite close to the pCO_2 values from SOCAT v2020 samples (Fig. 7).

Comparing the results based on a different combination of predictors, the results of FFNN1 (based on stepwise FFNN algorithm，this paper) and FFNN3 (based on 15 predictors from Denvil-Sommer et al. 2019) were more precise than that of FFNN2 (based on 10 predictors from Landschützer et al. 2014). The plots in the result of FFNN1 were most concentrated along the y=x line, suggesting extremely close FFNN outputs with the measured pCO_2 values from SOCAT, with the RMSE of 17.99 μatm in the global open oceans. The RMSE of FFNN1 was lower than that of FFNN2 (22.95 μatm) and FFNN3 (19.17 μatm).

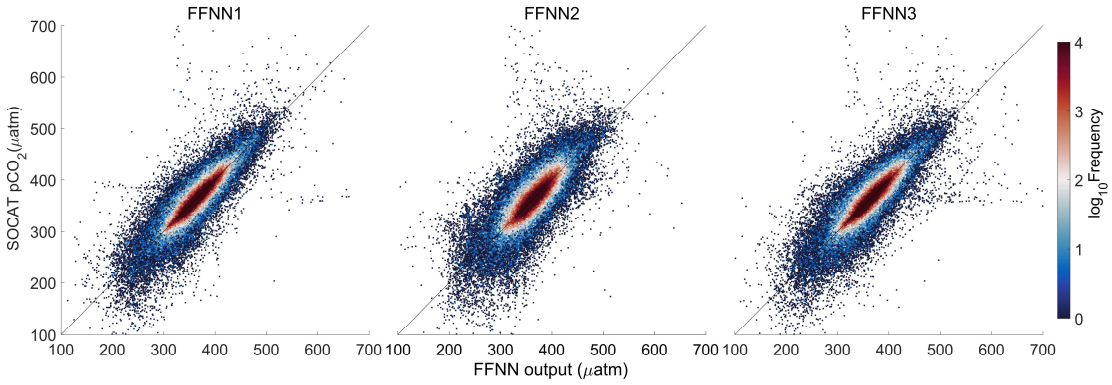

Figure 7. Comparison of FFNN predicted pCO_2 with SOCAT pCO_2. FFNN1 was based on predictors selected by the stepwise-FFNN algorithm. FFNN2 and FFNN3 were based on predictors from Landschützer et al., 2014 and Denvil-Sommer et al., 2019, respectively.

For specific comparison of accuracy in each province, the MAE of FFNN1 was lower in most provinces (Table 4), except for the relatively close results between the FFNN1 and FFNN3 in parts of provinces. The MAE of FFNN1 in the province P9 Indian Ocean was significantly lower than that of the other validation groups, suggesting a better combination of predictors highly related to the drivers of surface ocean pCO_2 and its variability in the Indian Ocean. Compared with FFNN2 and FFNN3, the predictors of FFNN1 added surface pressure and W velocity of ocean currents and abandoned the monthly anomalies of other predictors in the province P9 Indian Ocean. The low relevance between pCO_2 and part of the monthly anomalies, such as SSS_{anom} and SST_{anom}, may be responsible for significantly lower MAE of FFNN1. Adding redundant predictors may cause misleading in the learning of the FFNN model on the contrary. The MAE and RMSE differences between FFNN1 and FFNN3 in some provinces were relatively small. The reason for higher MAE and RMSE of FFNN2 may be applying latitudes and longitudes as predictors in both the FFNN1 and FFNN3 but not in the FFNN2. In the province P10 subpolar Southern Ocean, latitudes and longitudes were considered not good predictors by the stepwise FFNN algorithm, and

the results of three validation groups were extremely close.

Table 4. Performance of the pCO_2 prediction based on different predictors

Province	FFNN size	MAE (μatm)			RMSE (μatm)		
		FFNN1	FFNN2	FFNN3	FFNN1	FFNN2	FFNN3
P1 Arctic Ocean (9856)	10	**24.50**	32.32	26.87	**32.27**	43.68	35.08
P2 subpolar Pacific (30516)	35	**16.32**	20.63	16.67	**24.32**	29.87	25.03
P3 north subtropical Pacific (56367)	25	**7.39**	12.16	7.95	**11.33**	17.75	11.88
P4 subpolar Atlantic (29595)	10	**13.89**	16.91	14.73	**21.06**	24.29	22.27
P5 north subtropical Atlantic (45358)	35	**8.55**	12.28	9.00	**12.80**	17.86	13.72
P6 south Pacific (31803)	20	**6.96**	9.94	7.24	**9.86**	14.64	11.00
P7 equatorial Pacific (11233)	25	**15.05**	19.55	15.49	**20.98**	27.61	21.10
P8 south Pacific (10259)	25	**11.19**	15.07	12.43	**17.10**	20.87	17.66
P9 Indian Ocean (7440)	25	**11.54**	13.78	15.49	**17.15**	22.89	28.29
P10 subpolar Southern Ocean (21206)	15	**11.00**	11.76	12.14	**16.61**	17.22	17.66
P11 Southern Ocean ice (10683)	10	**24.84**	29.26	25.74	**34.73**	40.42	35.22
Global (264316)		**11.32**	15.08	12.06	**17.99**	22.95	19.17

(FFNN1 was based on predictors selected by the stepwise-FFNN algorithm. FFNN2 and FFNN3 were based on predictors from Landschützer et al., 2014 and Denvil-Sommer et al., 2019, respectively. The lowest MAE and RMSE between different validation groups was shown in bold.)

3.4 Validation based on independent observations

The FFNN outputs based on a different combination of predictors were compared with independent observations from the Ocean Time-series (HOT) (Dore et al., 2009), Bermuda Atlantic Time-series Study (BATS) (Bates, 2007), and The European Station for Time Series in the Ocean Canary Islands (ESTOC) (González-Dávila and Santana-Casiano, 2009) (Fig. 8). Compared with the independent observations from the HOT station, the three validation groups both show close results, which were also similar in the seasonal and interannual variability of pCO_2. From 1992 to 2019, the RMSE between FFNN1 outputs and HOT observations was only 9.29 μatm, lower than the 10.85 μatm of FFNN2 and the 10.70 μatm of FFNN3. The monthly mean pCO_2 of FFNN2 during winter was lower than the HOT observations and pCO_2 values of other validation groups, while the FFNN1 and FFNN3 outputs were closer to the HOT observations. MAE between predicted pCO_2 and HOT observations was also lower in the validation group FFNN1, which was only 7.17 μatm, compared to the 8.61 μatm of

FFNN2 and the 8.44 μatm of FFNN3. Higher bias generated in the winter bottom and summer peak, shown more obviously in the monthly average of pCO_2 (Fig. 8b). Compared with other validation groups, the result of FFNN1 was closer to the monthly average values of the HOT observations. The same conclusion can be obtained in the ESTOC and BATS station located in the province P5 north subtropical Atlantic. The RMSE between FFNN1 outputs and independent observations was 13.03 μatm in the BATS station and 11.35 μatm in the ESTOC station, lower than other validation groups. The RMSE between FFNN2 outputs and independent observations was 16.15 μatm in the BATS station and 14.51 μatm in the ESTOC station. For the group FFNN3, the RMSE was 13.09 μatm in the BATS station and 13.01 μatm in the ESTOC station. All results were extremely close to the independent observations, but the RMSE and MAE of FFNN1 were lower. Similar to the situation in the HOT station, the FFNN1 was most close and the FFNN3 second. Based on the better performance of FFNN1, in which the predictors selected by stepwise FFNN algorithm were used, we may conclude that the stepwise FFNN algorithm can effectively find a better combination of predictors to fit the diver of surface ocean pCO_2 and obtain a lower error.

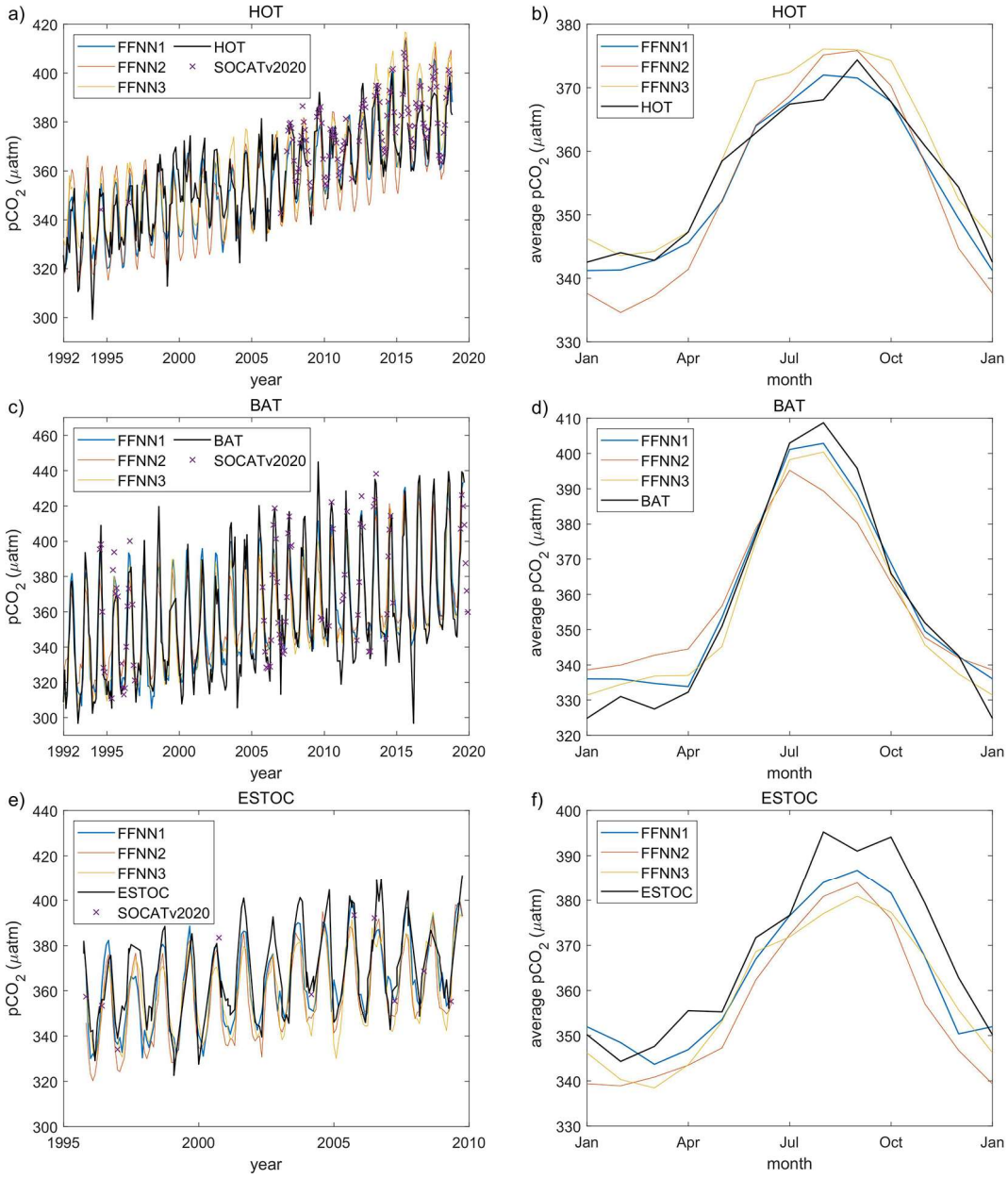

Figure 8. Validation based on independent observation from time series stations. a) and b): the Hawaii Ocean Time-series (HOT) (Dore et al., 2009); c) and d): the Bermuda Atlantic Time-series Study (BATS) (Bates, 2007); e) and f): the European Station for Time Series in the Ocean Canary Islands (ESTOC) (González-Dávila and Santana-Casiano, 2009) time-series station. FFNN1 was based on predictors selected by the stepwise-FFNN algorithm. FFNN2 and FFNN3 were based on predictors from Landschützer et al., 2014 and Denvil-Sommer et al., 2019, respectively. SOCATv2020 represents the monthly mean pCO_2 of SOCAT observations in the corresponding grids of each time series station.

3.5 Climatological spatial distribution

The climatological average distribution of pCO_2 suggested a significant spatial

variability (Fig. 9), consistent with the average distribution of SOCAT observations. In the Pacific Ocean, the high pCO_2 areas showed by the stepwise-FFNN product (Fig. 9b), including the equatorial areas, east temperate areas, and north subpolar areas, were highly consistent with the SOCAT datasets (Fig. 9a). Similarly, the distribution of pCO_2 in the Atlantic Ocean was also close. However, the stepwise-FFNN product suggested lower pCO_2 average values in the Arctic and higher values in the Southern Ocean near the Antarctic continent. Compared with the previous climatology product (Landschützer et al., 2020), the stepwise FFNN product has similar spatial patterns with high pCO_2 in the eastern equatorial Pacific and equatorial Atlantic: inconsistent spatial distribution also existed in the Arctic and parts of the Southern Ocean near the Antarctic continent. The differences between the stepwise-FFNN product and the previous climatology product may be caused by differences in methods or SOCAT dataset versions used. In comparison, lower average values of the SOCAT dataset in the Southern Ocean may be caused by the undersampling in winter. The global spatial distribution pattern of the stepwise FFNN pCO_2 product was basically well consistent with previous climatology product and SOCAT dataset, suggesting that pCO_2 predicting based on regional specific predictors selected by the stepwise FFNN algorithm was better than that based on the globally same predictors.

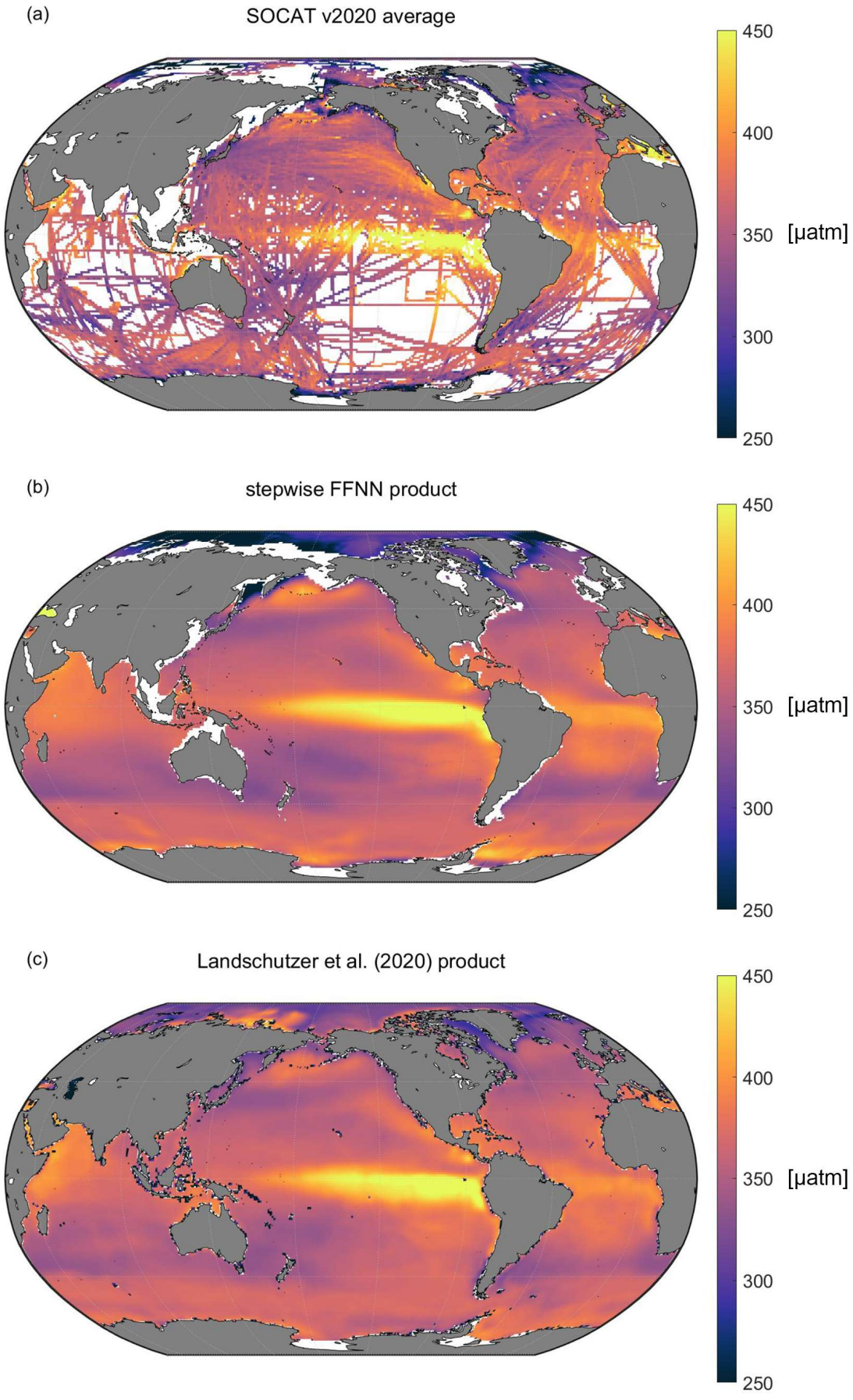
(a)
SOCAT v2020 average
450
400
350
300
250
[µatm]
(b)
stepwise FFNN product
450
400
350
300
250
[µatm]
(c)
Landschutzer et al. (2020) product
450
400
350
300
250
[µatm]

472

Figure 9. Comparison between long term average of a): SOCAT v2020 dataset, b): the stepwise FFNN pCO_2 product, and c): previous climatology product adapted from Landschützer et al., 2020.

4. Conclusions

A stepwise FFNN algorithm was constructed to decrease the predicting error in the surface ocean pCO_2 mapping by finding better combinations of pCO_2 predictors in each biogeochemical province defined by SOM method, based on which a monthly 1°×1° gridded global open-oceanic surface ocean pCO_2 product from January 1992 to August 2019 was constructed. Our work provided a statistical way of predictor selection for all researches based on relationship fitting by machine learning methods. The validation based on the SOCAT dataset and independent observations shows that using regional-specific predictors selected by the stepwise FFNN algorithm retrieved lower predicting error than globally same predictors. This stepwise FFNN algorithm can also be used in pCO_2 mapping research for higher resolution and coastal regions and other data mapping research using SOM or other region dividing methods. The preparation work was only collecting as many predictors, which are possibly related to the target data and need to be sufficiently available in time and space. However, high predicting error in particular regions remains to be improved, such as polar regions and equatorial Pacific. Since the stepwise FFNN algorithm's result largely depends on how biogeochemical provinces are divided, improving the SOM step is still necessary. Besides, the FFNN can be replaced by any suitable type of neural network. A possible way to improve the performance of the stepwise FFNN algorithm is to modify the structure of FFNN or to use networks with more sophisticated architecture and to use different learning algorithms. In the future work, the stepwise FFNN algorithm with possible improvement will be attempted in the mapping of other products, such as total alkalinity and pH, to provide sufficient data support for studies on ocean acidification and carbon cycling.

Code and data availability

The stepwise FFNN algorithm (as a .m file for MATLAB) and the global 1°×1° gridded surface ocean pCO_2 product since from January 1992 to August 2019 (as a NetCDF file) generated during this study is available from the Institute of Oceanology of the Chinese Academy of Sciences Marine Science Data Center at http://dx.doi.org/10.12157/iocas.2021.0022 or directly at http://english.casodc.com/data/metadata-special-detail?id=1418424272359075841 .

Author contribution

Ma Jun, Yuan Huamao and Duan Liqin collected the dataset of pCO_2 predictors, and Qu baoxiao and Wang Yanjun was contributed in the synthesis of datasets. Zhong Guorong, Li Xuegang and Song Jinming designed the predictor selection algorithm and performed the reconstruction of pCO_2 product. Wang Fan, Zhang Bin, Sun Xiaoxia, Zhang Wuchang, and Wang Zhenyan were contributed in the further improving. Zhong Guorong prepared the manuscript with contributions from all co-authors.

Competing interests

The authors declare that they have no conflict of interest.

Acknowledgement

This work was supported by The National Key Research and Development Program of China (No. 2017YFA0603204), the Strategic Priority Research Program of the Chinese Academy of Sciences (No. XDA19060401), National Natural Science Foundation of China (No. 91958103 and No. 42176200), and Natural Science Foundation of Shandong Province (ZR2020YQ28). We thank SOCAT for sharing the fCO_2 observation data. The Surface Ocean CO_2 Atlas (SOCAT) is an international effort, endorsed by the International Ocean Carbon Coordination Project (IOCCP), the Surface Ocean Lower Atmosphere Study (SOLAS) and the Integrated Marine Biosphere Research (IMBeR) program, to deliver a uniformly quality-controlled surface ocean CO_2 database. The many researchers and funding agencies responsible for the collection of data and quality control are thanked for their contributions to SOCAT. We thank NASA Goddard Space Flight Center, Ocean Ecology Laboratory, Ocean Biology Processing Group for sharing the Chlorophyll concentration data.

References

Bakker, D. C. E., Pfeil, B., Landa, C. S., Metzl, N., O'Brien, K. M., Olsen, A., Smith, K., Cosca, C., Harasawa, S., Jones, S. D., Nakaoka, S.-i., Nojiri, Y., Schuster, U., Steinhoff, T., Sweeney, C., Takahashi, T., Tilbrook, B., Wada, C., Wanninkhof, R., Alin, S. R., Balestrini, C. F., Barbero, L., Bates, N. R., Bianchi, A. A., Bonou, F., Boutin, J., Bozec, Y., Burger, E. F., Cai, W.-J., Castle, R. D., Chen, L., Chierici, M., Currie, K., Evans, W., Featherstone, C., Feely, R. A., Fransson, A., Goyet, C., Greenwood, N., Gregor, L., Hankin, S., Hardman-Mountford, N. J., Harlay, J., Hauck, J., Hoppema, M., Humphreys, M. P., Hunt, C., Huss, B., Ibanhez, J. S. P., Johannessen, T., Keeling, R., Kitidis, V., Koertzinger, A., Kozyr, A., Krasakopoulou, E., Kuwata, A., Landschützer, P., Lauvset, S. K., Lefevre, N., Lo Monaco, C., Manke, A., Mathis, J. T., Merlivat, L., Millero, F. J., Monteiro, P. M. S., Munro, D. R., Murata, A., Newberger, T., Omar, A. M., Ono, T., Paterson, K., Pearce, D., Pierrot, D., Robbins, L. L., Saito, S., Salisbury, J., Schlitzer, R., Schneider, B., Schweitzer, R., Sieger, R., Skjelvan, I., Sullivan, K. F., Sutherland, S. C., Sutton, A. J., Tadokoro, K., Telszewski, M., Tuma, M., van Heuven, S. M. A. C., Vandemark, D., Ward, B., Watson, A. J., and Xu, S.: A multi-decade record of high-quality fCO_2 data in version 3 of the Surface Ocean CO_2 Atlas (SOCAT), Earth System Science Data, 8, 383-413, 10.5194/essd-8-383-2016, 2016.

Bates, N. R.: Interannual variability of the oceanic CO_2 sink in the subtropical gyre of the North Atlantic Ocean over the last 2 decades, Journal of Geophysical Research: Oceans, 112, 2007.

Broullón, D., Pérez, F. F., Velo, A., Hoppema, M., Olsen, A., Takahashi, T., Key, R. M., Tanhua, T., González-Dávila, M., Jeansson, E., Kozyr, A., and van Heuven, S. M. A. C.: A global monthly climatology of total alkalinity: a neural network approach, Earth System Science Data, 11, 1109-1127, 10.5194/essd-11-1109-2019, 2019.

Broullon, D., Perez, F. F., Velo, A., Hoppema, M., Olsen, A., Takahashi, T., Key, R. M., Tanhua, T., Magdalena Santana-Casiano, J., and Kozyr, A.: A global monthly climatology of oceanic total dissolved inorganic carbon: a neural network approach, Earth System Science Data, 12, 1725-1743, 10.5194/essd-12-1725-2020, 2020.

Chen, L. Q., Xu, S. Q., Gao, Z. Y., Chen, H. Y., Zhang, Y. H., Zhan, J. Q., and Li, W.: Estimation of monthly air-sea CO_2 flux in the southern Atlantic and Indian Ocean using in-situ and remotely sensed data, Remote Sensing of Environment, 115, 1935-1941, 10.1016/j.rse.2011.03.016, 2011.

Cheng L. and J. Zhu: Benefits of CMIP5 multimodel ensemble in reconstructing historical ocean subsurface temperature variation, Journal of Climate, 29(15), 5393–5416, 10.1175/JCLI-D-15-0730.1, 2016.

Cheng L., K. Trenberth, J. Fasullo, T. Boyer, J. Abraham, J. Zhu: Improved estimates of ocean heat content from 1960 to 2015, Science Advances, 3, e1601545, 2017.

Cheng L., K. E. Trenberth, N. Gruber, J. P. Abraham, J. Fasullo, G. Li, M. E. Mann, X. Zhao, Jiang Zhu: Improved estimates of changes in upper ocean salinity and the hydrological cycle. Journal of Climate, 33, 10357–10381, 10.1175/JCLI-D-20-0366.1, 2020.

Chen, S., Hu, C., Barnes, B. B., Wanninkhof, R., Cai, W.-J., Barbero, L., and Pierrot, D.: A machine learning approach to estimate surface ocean pCO_2 from satellite measurements, Remote Sensing of Environment, 228, 203-226, 10.1016/j.rse.2019.04.019, 2019.

Chen, S. L., Hu, C. M., Byrne, R. H., Robbins, L. L., and Yang, B.: Remote estimation of surface pCO_2 on the West Florida Shelf, Continental Shelf Research, 128, 10-25, 10.1016/j.csr.2016.09.004, 2016.

Chen, S. L., Hu, C. M., Cai, W. J., and Yang, B.: Estimating surface pCO_2 in the northern Gulf of Mexico: Which remote sensing model to use?, Continental Shelf Research, 151, 94-110, 10.1016/j.csr.2017.10.013, 2017.

Commerce, U. D. o., Administration, N. O. a. A., and Center, N. G. D.: 2-minute Gridded Global Relief Data (ETOPO2v2). http://www.ngdc.noaa.gov/mgg/fliers/06mgg01.html, 2006.

Dee, D. P., Uppala, S. M., Simmons, A. J., Berrisford, P., Poli, P., Kobayashi, S., Andrae, U., Balmaseda, M. A., Balsamo, G., Bauer, P., Bechtold, P., Beljaars, A. C. M., van de Berg, L., Bidlot, J., Bormann, N., Delsol, C., Dragani, R., Fuentes, M., Geer, A. J., Haimberger, L., Healy, S. B., Hersbach, H., Holm, E. V., Isaksen, L., Kallberg, P., Kohler, M., Matricardi, M., McNally, A. P., Monge-Sanz, B. M., Morcrette, J. J., Park, B. K., Peubey, C., de Rosnay, P., Tavolato, C., Thepaut, J. N., and Vitart, F.: The

ERA-Interim reanalysis: configuration and performance of the data assimilation system, Q J Roy Meteor Soc, 137, 553-597, 10.1002/qj.828, 2011.

Denvil-Sommer, A., Gehlen, M., Vrac, M., and Mejia, C.: LSCE-FFNN-v1: a two-step neural network model for the reconstruction of surface ocean pCO_2 over the global ocean, Geoscientific Model Development, 12, 2091-2105, 10.5194/gmd-12-2091-2019, 2019.

Dore, J. E., Lukas, R., Sadler, D. W., Church, M. J., and Karl, D. M.: Physical and biogeochemical modulation of ocean acidification in the central North Pacific, Proceedings of the National Academy of Sciences, 106, 12235-12240, 2009.

Friedlingstein, P., Jones, M. W., O'Sullivan, M., Andrew, R. M., Hauck, J., Peters, G. P., Peters, W., Pongratz, J., Sitch, S., Le Quere, C., Bakker, D. C. E., Canadell, J. G., Ciais, P., Jackson, R. B., Anthoni, P., Barbero, L., Bastos, A., Bastrikov, V., Becker, M., Bopp, L., Buitenhuis, E., Chandra, N., Chevallier, F., Chini, L. P., Currie, K. I., Feely, R. A., Gehlen, M., Gilfillan, D., Gkritzalis, T., Goll, D. S., Gruber, N., Gutekunst, S., Harris, I., Haverd, V., Houghton, R. A., Hurtt, G., Ilyina, T., Jain, A. K., Joetzjer, E., Kaplan, J. O., Kato, E., Goldewijk, K. K., Korsbakken, J. I., Landschützer, P., Lauvset, S. K., Lefevre, N., Lenton, A., Lienert, S., Lombardozzi, D., Marland, G., McGuire, P. C., Melton, J. R., Metzl, N., Munro, D. R., Nabel, J. E. M. S., Nakaoka, S.-I., Neill, C., Omar, A. M., Ono, T., Peregon, A., Pierrot, D., Poulter, B., Rehder, G., Resplandy, L., Robertson, E., Rodenbeck, C., Seferian, R., Schwinger, J., Smith, N., Tans, P. P., Tian, H., Tilbrook, B., Tubiello, F. N., van der Werf, G. R., Wiltshire, A. J., and Zaehle, S.: Global Carbon Budget 2019, Earth System Science Data, 11, 1783-1838, 10.5194/essd-11-1783-2019, 2019.

Friedrich, T., and Oschlies, A.: Neural network-based estimates of North Atlantic surface pCO_2 from satellite data: A methodological study, Journal of Geophysical Research-Oceans, 114, Artn C03020, 10.1029/2007jc004646, 2009.

Garcia, H., Weathers, K., Paver, C., Smolyar, I., Boyer, T., Locarnini, M., Zweng, M., Mishonov, A., Baranova, O., and Seidov, D.: World Ocean Atlas 2018. Vol. 4: Dissolved Inorganic Nutrients (phosphate, nitrate and nitrate+ nitrite, silicate), 2019a.

Garcia, H., Weathers, K., Paver, C., Smolyar, I., Boyer, T., Locarnini, M., Zweng, M., Mishonov, A., Baranova, O., and Seidov, D.: World Ocean Atlas 2018, Volume 3: Dissolved Oxygen, Apparent Oxygen Utilization, and Dissolved Oxygen Saturation, 2019b.

GLOBALVIEW-CO2: Cooperative Atmospheric Data Integration Project - Carbon Dioxide [CD-ROM]. NOAA ESRL, B., Colo. (Ed.), [Available at ftp.cmdl.noaa.gov, path: ccg/co2/GLOBALVIEW, 5th January 2013.], 2011.

González-Dávila, M., and Santana-Casiano, J.: Sea surface and atmospheric fCO_2 data measured during the estoc time series cruises from 1995-2009, CDIAC, Oak Ridge National Laboratory, US Department of Energy, Oak Ridge, Tennessee. doi, 10, 2009.

Gregor, L., Lebehot, A. D., Kok, S., & Scheel Monteiro, P. M. A comparative assessment of the uncertainties of global surface ocean CO_2 estimates using a machine-learning ensemble (CSIR-ML6 version 2019a)–have we hit the wall?. Geoscientific Model Development, 12(12), 5113-5136, 2019.

Hales, B., Strutton, P. G., Saraceno, M., Letelier, R., Takahashi, T., Feely, R., Sabine, C., and Chavez, F.: Satellite-based prediction of pCO_2 in coastal waters of the eastern North Pacific, Prog Oceanogr, 103, 1-15, 10.1016/j.pocean.2012.03.001, 2012.

Huang, B., Thorne, P. W., Banzon, V. F., Boyer, T., Chepurin, G., Lawrimore, J. H., Menne, M. J., Smith, T. M., Vose, R. S., and Zhang, H.-M.: Extended reconstructed sea surface temperature, version 5 (ERSSTv5): upgrades, validations, and intercomparisons, J Climate, 30, 8179-8205, 2017.

Iida, Y., Kojima, A., Takatani, Y., Nakano, T., Midorikawa, T., and Ishii, M.: Trends in pCO_2 and sea-air CO_2 flux over the global open oceans for the last two decades, J. Oceanogr., 71, 637–661, 10.1007/s10872-015-0306-4, 2015.

Jo, Y. H., Dai, M. H., Zhai, W. D., Yan, X. H., and Shang, S. L.: On the variations of sea surface pCO_2 in the northern South China Sea: A remote sensing based neural network approach, Journal of Geophysical Research-Oceans, 117, Artn C08022, 10.1029/2011jc007745, 2012.

Körtzinger, A.: Determination of carbon dioxide partial pressure (pCO_2), 3rd ed., Methods of Seawater Analysis, 3rd edn., 1999.

Landschützer, P., Gruber, N., Bakker, D. C. E., and Schuster, U.: Recent variability of the global ocean carbon sink, Glob. Biogeochem. Cycle, 28, 927-949, 10.1002/2014gb004853, 2014.

Landschützer, P., Gruber, N., Bakker, D. C. E., Schuster, U., Nakaoka, S., Payne, M. R., Sasse, T. P., and Zeng, J.: A neural network-based estimate of the seasonal to inter-annual variability of the Atlantic Ocean carbon sink, Biogeosciences, 10, 7793-7815, 10.5194/bg-10-7793-2013, 2013.

Landschützer, P., Gruber, N., and Bakker, D. C. E.: Decadal variations and trends of the global ocean carbon sink, Glob. Biogeochem. Cycle, 30, 1396-1417, 10.1002/2015gb005359, 2016.

Landschützer, P., Laruelle, G. G., Roobaert, A., and Regnier, P.: A uniform pCO_2 climatology combining open and coastal oceans, Earth Syst. Sci. Data Discuss., 2020, 1-30, 10.5194/essd-2020-90, 2020.

Laruelle, G. G., Landschützer, P., Gruber, N., Tison, J. L., Delille, B., and Regnier, P.: Global high-resolution monthly pCO_2 climatology for the coastal ocean derived from neural network interpolation, Biogeosciences, 14, 4545-4561, 10.5194/bg-14-4545-2017, 2017.

Marrec, P., Cariou, T., Mace, E., Morin, P., Salt, L. A., Vernet, M., Taylor, B., Paxman, K., and Bozec, Y.: Dynamics of air-sea CO_2 fluxes in the northwestern European shelf based on voluntary observing ship and satellite observations, Biogeosciences, 12, 5371-5391, 10.5194/bg-12-5371-2015, 2015.

Marshall G J.: Trends in the Southern Annular Mode from observations and reanalyses, Journal of climate, 16, 10.1175/1520-0442(2003)016<4134:TITSAM>2.0.CO;2, 4134-4143, 2003.

Menemenlis, D., Campin, J.-M., Heimbach, P., Hill, C., Lee, T., Nguyen, A., Schodlok, M., and Zhang, H.: ECCO2: High Resolution Global Ocean and Sea Ice Data Synthesis, Mercator Ocean Quarterly Newsletter, 2008.

Moussa, H., Benallal, M. A., Goyet, C., and Lefevre, N.: Satellite-derived CO_2 fugacity in surface seawater of the tropical Atlantic Ocean using a feedforward neural network, Int J Remote Sens, 37, 580-598, 10.1080/01431161.2015.1131872, 2016.

Nakaoka, S., Telszewski, M., Nojiri, Y., Yasunaka, S., Miyazaki, C., Mukai, H., and Usui, N.: Estimating temporal and spatial variation of ocean surface pCO_2 in the North Pacific using a self-organizing map neural network technique, Biogeosciences, 10, 6093-6106, 10.5194/bg-10-6093-2013, 2013.

NASA Goddard Space Flight Center, Ocean Ecology Laboratory, Ocean Biology Processing Group. Moderate-resolution Imaging Spectroradiometer (MODIS) Aqua Chlorophyll Data; 2018 Reprocessing. NASA OB.DAAC, Greenbelt, MD, USA. 10.5067/AQUA/MODIS/L3M/CHL/2018, 2018.

Rödenbeck, C., Bakker, D. C. E., Metzl, N., Olsen, A., Sabine, C., Cassar, N., Reum, F., Keeling, R. F., and Heimann, M.: Interannual sea–air CO_2 flux variability from an observationdriven ocean mixed-layer scheme, Biogeosciences, 11, 4599–4613, 10.5194/bg-11-4599-2014, 2014.

Sabine, C. L., Feely, R. A., Gruber, N., Key, R. M., Lee, K., Bullister, J. L., Wanninkhof, R., Wong, C. S., Wallace, D. W. R., Tilbrook, B., Millero, F. J., Peng, T. H., Kozyr, A., Ono, T., and Rios, A. F.: The oceanic sink for anthropogenic CO_2, Science, 305, 367-371, DOI 10.1126/science.1097403, 2004.

Sarma, V. V. S. S., Saino, T., Sasaoka, K., Nojiri, Y., Ono, T., Ishii, M., Inoue, H. Y., and Matsumoto, K.: Basin-scale pCO_2 distribution using satellite sea surface temperature, Chl-a, and climatological salinity in the North Pacific in spring and summer, Glob. Biogeochem. Cycle, 20, Artn Gb3005, 10.1029/2005gb002594, 2006.

Shadwick, E. H., Thomas, H., Comeau, A., Craig, S. E., Hunt, C. W., and Salisbury, J. E.: Air-Sea CO_2 fluxes on the Scotian Shelf: seasonal to multi-annual variability, Biogeosciences, 7, 3851-3867, 10.5194/bg-7-3851-2010, 2010.

Signorini, S. R., Mannino, A., Najjar, R. G., Friedrichs, M. A. M., Cai, W. J., Salisbury, J., Wang, Z. A., Thomas, H., and Shadwick, E.: Surface ocean pCO_2 seasonality and sea-air CO_2 flux estimates for the North American east coast, Journal of Geophysical Research-Oceans, 118, 5439-5460, 10.1002/jgrc.20369, 2013.

Takahashi, T., Sutherland, S. C., Feely, R. A., and Wanninkhof, R.: Decadal change of the surface water pCO_2 in the North Pacific: A synthesis of 35 years of observations, Journal of Geophysical Research-Oceans, 111, Artn C07s05, 10.1029/2005jc003074, 2006.

Takahashi, T., Sutherland, S. C., Wanninkhof, R., Sweeney, C., Feely, R. A., Chipman, D. W., Hales, B., Friederich, G., Chavez, F., Sabine, C., Watson, A., Bakker, D. C. E., Schuster, U., Metzl, N., Yoshikawa-Inoue, H., Ishii, M., Midorikawa, T., Nojiri, Y., Kortzinger, A., Steinhoff, T., Hoppema, M., Olafsson, J., Arnarson, T. S., Tilbrook, B., Johannessen, T., Olsen, A., Bellerby, R., Wong, C. S., Delille, B., Bates, N. R., and de Baar, H. J. W.: Climatological mean and decadal change in surface ocean pCO_2, and net sea-air CO_2 flux over the global oceans, Deep-Sea Research Part Ii-Topical Studies in Oceanography, 56, 554-577, 10.1016/j.dsr2.2008.12.009, 2009.

Telszewski, M., Chazottes, A., Schuster, U., Watson, A. J., Moulin, C., Bakker, D. C. E., Gonzalez-Davila, M., Johannessen, T., Kortzinger, A., Luger, H., Olsen, A., Omar, A., Padin, X. A., Rios, A. F., Steinhoff, T., Santana-Casiano, M., Wallace, D. W. R., and Wanninkhof, R.: Estimating the monthly pCO_2 distribution in the North Atlantic using a self-organizing neural network, Biogeosciences, 6, 1405-1421, DOI 10.5194/bg-6-1405-2009, 2009.

Wang, Y., Li, X., Song, J., Zhong, G., and Zhang, B.: Carbon Sinks and Variations of pCO_2 in the Southern Ocean from 1998 to 2018 Based on a Deep Learning Approach, IEEE Journal of Selected Topics in Applied Earth Observations and Remote Sensing, 2021.

Watson, A. J., Schuster, U., Shutler, J. D., Holding, T., Ashton, I. G. C., Landschützer, P., Woolf, D. K., and Goddijn-Murphy, L.: Revised estimates of ocean-atmosphere CO_2 flux are consistent with ocean carbon inventory, Nature Communications, 11, 10.1038/s41467-020-18203-3, 2020.

Weiss, R. F.: Carbon dioxide in water and seawater: the solubility of a non-ideal gas, Marine Chemistry, 2, 203--215, 1974.

Zeng, J., Nojiri, Y., Landschützer, P., Telszewski, M., and Nakaoka, S.: A Global Surface Ocean fCO_2 Climatology Based on a Feed-Forward Neural Network, Journal of Atmospheric and Oceanic Technology, 31, 1838-1849, 10.1175/jtech-d-13-00137.1, 2014.

Zeng, J. Y., Nojiri, Y., Nakaoka, S., Nakajima, H., and Shirai, T.: Surface ocean CO_2 in 1990-2011 modelled using a feed-forward neural network, Geosci Data J, 2, 47-51, 10.1002/gdj3.26, 2015.

Zeng, J. Y., Matsunaga, T., Saigusa, N., Shirai, T., Nakaoka, S., and Tan, Z. H.: Technical note: Evaluation of three machine learning models for surface ocean CO_2 mapping, Ocean Sci, 13, 303-313, 10.5194/os-13-303-2017, 2017.

Zhong, G., Li, X., Qu, B., Wang, Y., Yuan, H, and Song, J.: A General Regression Neural Network approach to reconstruct global 1°×1° resolution sea surface pCO_2, Acta Oceanol Sin, 10, 70-79, 10.3969/j.issn.0253-4193.2020.10.007, 2020.